ACS APPLIED MATERIALS & INTERFACES

Research Article

www.acsami.org

High Efficiency Hybrid Silicon Nanopillar–Polymer Solar Cells

Pushpa Raj Pudasaini,[†,*] Francisco Ruiz-Zepeda,[†] Manisha Sharma,[‡] David Elam,[†] Arturo Ponce,[†] and Arturo A. Ayon[†]

[†]Department of Physics and Astronomy and [‡]Department of Chemistry, University of Texas at San Antonio, One UTSA Circle, San Antonio, Texas 78249, United States

Supporting Information

ABSTRACT: Recently, inorganic/organic hybrid solar cells have been considered as a viable alternative for low-cost photovoltaic devices because the Schottky junction between inorganic and organic materials can be formed employing low temperature processing methods. We present an efficient hybrid solar cell based on highly ordered silicon nanopillars (SiNPs) and poly(3,4-ethylene-dioxythiophene):polystyrenesulfonate (PEDOT:PSS). The proposed device is formed by spin coating the organic polymer PEDOT:PSS on a SiNP array fabricated using metal assisted electroless chemical etching process. The characteristics of the hybrid solar cells are investigated as a function of SiNP height. A maximum power conversion efficiency (PCE) of 9.65% has been achieved for an optimized SiNP array hybrid solar cell with nanopillar height of 400 nm, despite the absence of a back surface field enhancement. The effect of an ultrathin atomic layer deposition (ALD), grown aluminum oxide (Al_2O_3), as a passivation layer (recombination barrier) has also been studied for the enhanced electrical performance of the device. With the inclusion of the ultrathin ALD deposited Al_2O_3 between the SiNP array textured surface and the PEDOT:PSS layer, the PCE of the fabricated device was observed to increase to 10.56%, which is ∼10% greater than the corresponding device without the Al_2O_3 layer. The device described herein is considered to be promising toward the realization of a low-cost, high-efficiency inorganic/organic hybrid solar cell.

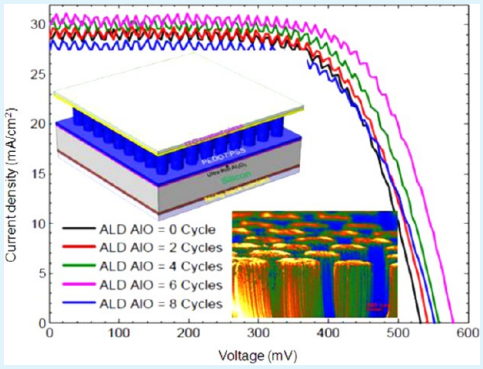

KEYWORDS: *solar cell, light trapping, heterojunction, conductive polymer, silicon nanopillars, radial junction*

INTRODUCTION

Crystalline silicon (c-Si) has enjoyed years of success in the photovoltaic industry due to its relatively high power conversion efficiencies (PCEs).[1−4] In addition, it exhibits other advantages such as high abundance, nontoxicity, and well-established processing technologies. Nonetheless, photovoltaic devices based on c-Si are relatively expensive compared to other photovoltaic technologies, mainly due to the relatively complex high temperature fabrication steps involved, as well as the required thickness of the c-Si wafer to absorb most of the solar spectrum due to its indirect band gap. On the other hand, organic photovoltaic (OPV) devices based on conjugated polymers, which can be fabricated by relatively simple, low temperature techniques utilizing inexpensive materials, have the potential for demonstrating low cost photovoltaic devices.[5−10] However, as of today, state-of-the-art organic solar cells exhibit relatively low PCE compared to their c-Si counterparts. One of the greatest challenges of OPV is the relative paucity of electron accepting materials which may be paired with hole conducting polymers to induce exciton dissociation at the interface. An interesting approach to this problem is to use semiconducting nanostructures as an electron accepting phase to form organic/inorganic hybrid solar cells. Therefore, hybrid solar cells based on inorganic semiconductors and organic conjugated polymers combine both of their advantages and provide a possible alternative route to enable low cost photovoltaic devices.[11−18] A commonly used organic material for hybrid PV devices is the conjugated polymer, poly(3,4-ethylene dioxythiophene):poly-(styrenesulfonate) (PEDOT:PSS), which is transparent and conductive (<1000 S/cm). Most of the incoming light is absorbed in the Si layer in Si/organic hybrid solar cells; thus, the PCE of the device, in principle, may be comparable to conventional Si p−n junction solar cells. However, to the best of our knowledge, the power conversion efficiencies of Si/organic polymer hybrid solar cells are relatively low (∼10%), compared to conventional c-Si solar cells.[13,14,19−22] Some of the challenges, such as excessive carrier recombination, decay of excitons within a diffusion length <10 nm, and interface carrier transport inside the polymer, cause serious limitations to the efficiency of the aforementioned Si/organic hybrid solar cells.[16,23−26] In order to address some of these issues, different groups have incorporated Si nanostructures like silicon nanowires (SiNWs), silicon nanocones (SiNCs), silicon nanopillars (SiNPs), etc. in the active polymer layer of a device.[19,21,27] Additionally, the vertically aligned SiNWs have been reported to exhibit excellent light absorption character-

Received: July 1, 2013
Accepted: September 13, 2013
Published: September 13, 2013

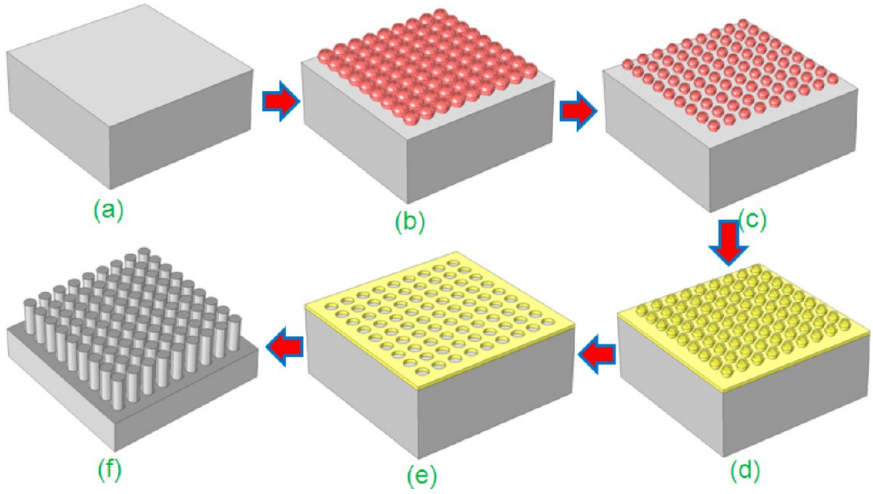

Figure 1. Schematic illustration of the fabrication process of a periodic SiNP array. (a) RCA clean of the n-type Si (100) wafer, (b) self-assembled monolayer of PS nanoparticles on the Si surface, (c) etch back of PS nanoparticles by using an O_2 plasma barrel etcher, (d) etched-back PS nanoparticles covered by a few nanometers of Au, (e) honeycomblike Au pattern on Si created by removing PS nanoparticles, and (f) periodic SiNP array fabricated by metal assisted chemical etching process.

istics both theoretically and experimentally.[3,28−32] However, there is still a challenge to fabricate a densely packed SiNW array with nanowire spacing close to the exciton diffusion length and synthesizing a conductive polymer having low exciton binding energy, which can fill the nanowire to form a core−shell structure. The commercially available PEDOT:PSS solution does not wet easily the highly hydrophobic SiNW array textured surface and the spacing between the nanowires is normally too small to be filled with the conductive polymer to form a core−shell heterojunction. Therefore, other organic compounds are frequently added to ensure a complete coverage on the highly dense vertical SiNW array. Furthermore, the performance of a SiNW/organic polymer hybrid solar cell depends on the surface/interface preparation. Carrier recombination at the surface/interface of the SiNWs due to their large surface to volume ratio is a major impediment for the efficient hybrid solar cell devices. To this end, the conductivity and wettability of PEDOT:PSS, the spin coating parameters (spin-casting speed and time) to control the thickness of the PEDOT:PSS layer on the textured Si surface, and the annealing temperature after the spin coating process could all influence the interface properties of a hybrid solar cell. A thin dielectric interface passivation layer between the Si and PEDOT:PSS layer could also have a significant effect on the PV performance of the proposed hybrid devices. Zhang et al.[33] have reported that compared to a hydrogen terminated silicon (−H−Si) surface, the short circuit current density (J_{SC}) of a planar Si/poly(3-hexylthiophene) (P3HT) hybrid cell with an oxygen terminated silicon (−SiO*x*−Si) surface exhibits a 200-fold enhancement. This has been attributed to the formation of a thin native oxide (SiO*x*) layer leading to the formation of a favorable internal electric field at the interface for an efficient carrier extraction. For the methyl terminated silicon (−CH_3−Si) surface decorated with platinum (Pt) nanodots, they reported a PCE as high as 5.9%. The effect of interfacial native oxide as a passivation layer (recombination barrier) on the electrical performance of a planar Si/PEDOT:PSS hybrid solar cell was studied by He et al.[34] A maximum power conversion efficiency of 10.6% was reported with a 1.5 nm interfacial SiO*x* layer between the Si (111) surface and the PEDOT:PSS layer. However, a thin native oxide layer is important but cannot be too large, because a thick oxide layer could create an insulating barrier for electrical transport, thereby deteriorating the solar cell performance. It was observed that PEDOT:PSS promotes for the oxidation of SiNP array textured surface thereby increasing the SiO*x* layer thickness over time. Therefore, the performance of a hybrid SiNP/PEDOT:PSS device deteriorates by aging. Moreover, Khatri et al. reported an enhanced electrical performance of a Si/PEDOT:PSS hybrid device with the incorporation of green-tea modified multiwall carbon nanotubes as an interface recombination barrier.[26] The investigation of determining the best passivating layer (recombination barrier) on a Si/PEDOT:PSS hybrid solar and the corresponding optimization is still underway.

In this paper, we report an efficient hybrid solar cell composed of a vertically aligned silicon nanopillar array (SiNP) and a PEDOT:PSS organic polymer employing an ultrathin ALD deposited Al_2O_3 passivation (barrier) layer. The relatively large spacing between the nanopillars, compared to the randomly oriented SiNWs fabricated by metal assisted electroless chemical etching, permitted a conformal polymer coating for the formation of a radial p−n junction. ALD Al_2O_3 was chosen as a passivation layer (recombination barrier) due to its unique chemical and field effect passivation characteristics, as well as the ability of ALD to deposit high quality, conformal films on high aspect ratio surfaces, with angstrom level control of the film thickness at low temperature. The influence of an interfacial Al_2O_3 layer on carrier collection efficiency is directly reflected on the measured photovoltaic performance of the device. The maximum short circuit current density (J_{SC}) and PCE values of 30.1 mA/cm^2 and 10.56%, respectively, were obtained for an optimized SiNPs/PEDOT:PSS solar cell with 6 cycles for the interfacial ALD Al_2O_3. For a thicker interfacial Al_2O_3 corresponding to an increased number of ALD cycles, the measured PCE of the device deteriorated due to a larger series resistance.

2. EXPERIMENTAL DETAILS

2.1. Silicon Nanopillar Array Fabrication. Highly ordered wafer scale SiNP arrays were fabricated by metal assisted electroless chemical etching in combination with nanosphere lithography. The detailed fabrication procedure can be found elsewhere.[35−37] Summarily, a 1−2

dx.doi.org/10.1021/am402598j | ACS Appl. Mater. Interfaces 2013, 5, 9620−9627

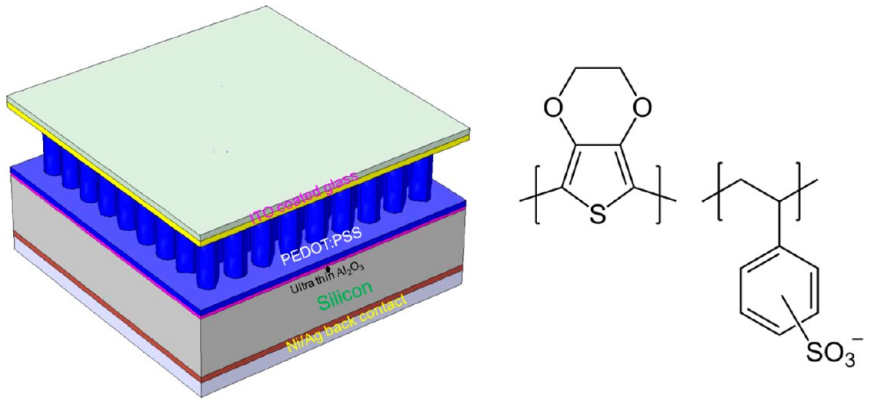

Figure 2. (a) Schematic illustration of the fabricated SiNP/PEDOT:PSS solar cell. (b) Chemical structure of PEDOT:PSS.

mL of polystyrene (PS) nanoparticle suspension with nanoparticle size of 650 nm (Duke Scientific, Palo Alto, CA) diluted with methanol and Triton X-100 was spin coated on a previously cleaned n-type silicon (100) wafer to form a self-assembled monolayer. The PS nanoparticle coated samples were exposed to an O_2 plasma in a commercial barrel etcher to shrink the size of PS particles. Then, a few nanometers of gold (Au) were deposited on the PS coated samples. A honeycomblike Au pattern on Si was then formed by removing the PS nanoparticles using sonication. Finally, the samples were immersed in an etching solution comprised of HF (49%), H_2O_2, and DI water in the volume ratio of 3:1:7 to form a periodic SiNP array textured surface. The height of the SiNPs can be controlled by varying the Si etching time. The underlying Au layer was subsequently removed by immersing the samples in a gold etchant solution (Sigma-Aldrich). The schematic fabrication process of periodic SiNPs array is shown in Figure 1.

2.2. Atomic Layer Deposition of Al_2O_3. The ALD of Al_2O_3 was carried out with a Cambridge Nanotech Savanah 200 system. The platen temperature was maintained at 110 °C during the deposition process. The precursors, trimethylaluminium (TMA) and water (H_2O), were kept at room temperature. Nitrogen (N_2) was used as a carrier and purging gas. ALD is a deposition process that employs cyclical self-limiting gas-surface reactions. This self-limiting reaction property is important for a conformal deposition in high aspect ratio structures due to the time required for the reactant gases to fully diffuse into the narrow channel. The average growth rate of this process estimated over 100 cycles on a blank Si (100) wafer with a native oxide as measured with ellipsometry was 1.1 Å/cycle. The index of refraction of the as deposited film was measured to be 1.71.

2.3. Device Fabrication. Prior to device fabrication, the produced SiNP array textured samples went through a rigorous cleaning procedure. At first, any polystyrene residues were removed by immersing the sample in a toluene solution (99.9%, Sigma-Aldrich) at 50 °C for 30 min. Second, the samples were cleaned by immersing them in a solution consisting of H_2O_2 (30%), NH_4OH (37%), and DI water in the volume ratio of 1:1:5 at 80 °C for 30 min to remove any other organic residues. The samples were transferred to a DI water bath for 10 min. Again, the samples were immersed in a solution comprised of H_2O_2 (30%), HCl (37%), and DI water in the volume ratio of 1:1:5 at 80 °C for 30 min to remove any metallic contamination. The samples were then transferred to a DI water bath for 10 min. Finally, the samples were cleaned in a diluted HF (2%) solution for 60 s to remove the native oxide. Immediately, the samples were transferred to the ALD chamber for the few cycles of Al_2O_3 deposition. Different samples were prepared with various thicknesses of Al_2O_3. Subsequently, 10 nm of nickel and 400 nm of silver were deposited on the back side and the samples were annealed at 425 °C for 30 min to form a rear contact. Highly conductive PEDOT:PSS (Sigma-Aldrich) mixed with dimethyl sulphoxide and Triton X-100 (surfactant) solution was spin-cast at 300 rpm for 10 s and 2000 rpm for 60 s to form a core−shell radial junction. The samples were then annealed on a hot plate at 140 °C for 10 min to remove the solvent. Finally, an ITO coated glass with a resistivity of 8−12 Ω (Sigma-Aldrich) was employed as a front contact to complete the cell. Each device had an active area of 1 cm^2. Different solar cell samples were also fabricated by the same procedure without the interfacial Al_2O_3 layer between the Si (100) surface and the PEDOT:PSS layer. Figure 2a depicts the schematic illustration of the fabrication of a SiNPs/PEDOT:PSS solar cells. The chemical structure of the PEDOT:PSS transparent conductive polymer is shown in Figure 2b.

2.4. Characterization. The morphology of the samples was collected by using high-resolution scanning electron microscopy (SEM) with a Field emission gun Hitachi S-5500. Transmission electron microscopy (TEM) was used to obtain high-resolution images at the Al_2O_3 and silicon interface in a JEOL 2010F TEM microscope operated at 200 kV. The cross-sectional TEM samples were prepared through a conventional mechanical polishing process including cutting, grinding, polishing, and a final ion milling thinning step. The optical reflectance spectra measurements were performed by using a UV−vis−NIR (Varian cary-5000) spectrometer equipped with integrating sphere. The PV measurement was performed using a solar simulator (Newport Sol2A) under AM 1.5 G illumination (1000 W/m^2) at standard testing conditions. Prior each sample measurement, the simulator intensity was calibrated with a reference cell from Newport (Irvine CA, USA) to ensure that the irradiation variation was within 3%. The external quantum efficiency (EQE) system used a 300 W xenon light source with a spot size of 1 mm × 3 mm and calibrated with a silicon photodetector also from Newport.

3. RESULTS AND DISCUSSION

3.1. Characterization of SiNP/Organic Hybrid Structure. Figure 3a includes a large SEM micrograph of the vertically aligned SiNP array (top view) fabricated by metal assisted electroless chemical etching methods. The same Figure 3a includes an inset in the upper right corner with higher magnification SEM micrographs of the same sample. Nanosphere lithography was employed to control the dimension of the SiNPs (diameter and interpillar spacing). The distance between the centers of any two pillars was fixed at 650 nm, and this value was determined by using PS nanoparticles with that particular diameter. The density of the SiNP array was measured to be ~2.7 × 10^6 pillars/mm^2. Since the opening between the pillars was ~200 nm, it was considered to be sufficient for the conformal coating of the SiNP array with PEDOT:PSS, without the addition of any organic molecules (see Supporting Information Figure S1). The inset in the lower left corner in Figure 3a shows the top view of PEDOT:PSS

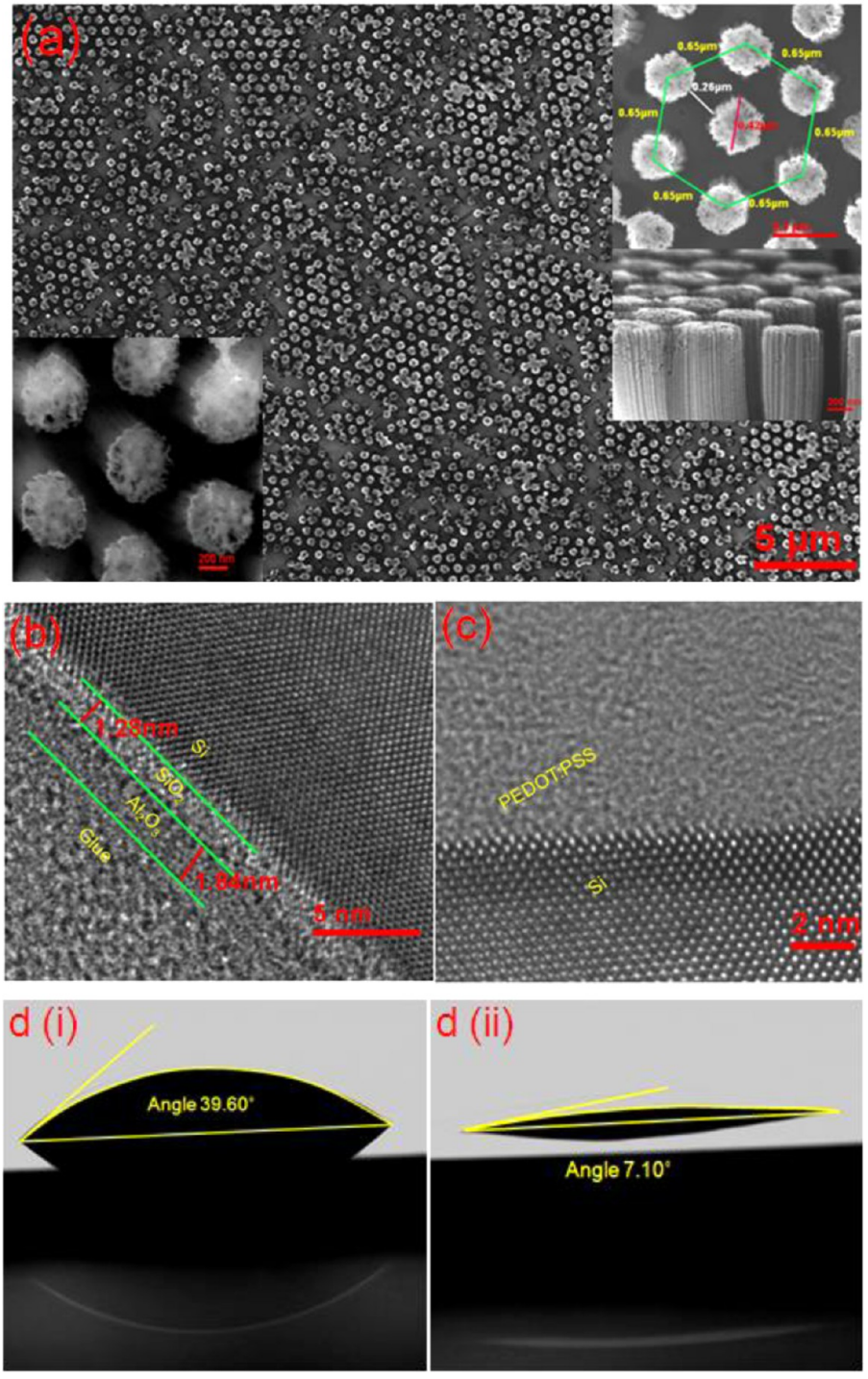

Figure 3. SEM micrographs of (a) top view of a SiNP array textured silicon surface; the inset on the upper right corner includes higher magnification images of the same sample, where it is possible to discern the hexagonal order of the SiNP array. The inset on the lower left corner shows a high magnification image of the SiNP array, coated with the transparent and conductive polymer PEDOT:PSS by spin-casting at 2000 rpm. (b) High resolution TEM micrograph of a 20-cycle ALD Al_2O_3 deposited on silicon at 170 °C, showing a 1.28 nm native oxide layer grown during the deposition process. (c) TEM image of the PEDOT:PSS on Si interface, with a 6-cycle ALD Al_2O_3 layer deposited at 110 °C without a discernible native oxide layer grown at the interface. (d) Photograph of an IPA-diluted PEDOT:PSS on (i) a hydrogen-terminated SiNP array textured surface (ii) and SiNP array textured surface coated with an ultrathin ALD Al_2O_3 layer, contrasting the different surface wettability.

coated SiNP array textured surface. The thickness of the PEDOT:PSS layer was approximately 40 nm. SiNP arrays with average heights of 200, 400, 800, and 1200 nm were fabricated by etching the sample for 30, 60, 120, and 180 s, respectively. The fabricated SiNP array samples underwent a rigorous cleaning procedure as described in a previous paragraph, followed by an HF dip for native oxide removal. The samples were then immediately transferred to the ALD chamber to deposit an ultrathin Al_2O_3 interface layer. Al_2O_3 deposition was carried out at the relatively low temperature of ∼110 °C to minimize native oxide growth. Longer time exposures at higher temperatures produce unacceptably thick native oxide interface

dx.doi.org/10.1021/am402598j | ACS Appl. Mater. Interfaces 2013, 5, 9620−9627

layers on the samples. Figure 3b shows the collected TEM image where it is possible to discern the native oxide layer with a thickness of ~1.28 nm, grown during 20 cycles of ALD Al_2O_3 deposition at 170 °C. Thicker interface layers impose higher barrier potentials for charge carriers to tunnel through, hindering the collection efficiency of the device. Therefore, we reduced the platen temperature and the number of cycles during ALD deposition to minimize the thickness of the native oxide layer grown at the interface. Figure 3c shows the TEM image of the PEDOT:PSS layer on a c-Si sample with an ultrathin (6 cycles) ALD Al_2O_3 deposited at 110 °C. The presence of an ultrathin Al_2O_3 at the interface between the Si and PEDOT:PSS is also confirmed by the EDX spectra obtained at the interface (see Supporting Information Figure S2). The EDX analysis was performed using an EDAX detector attached to a JEOL-ARM microscope operating at 200 kV. The deposition of a subnanometer Al_2O_3 also improves the wettability of PEDOT:PSS on the SiNP array textured surface (see Figure 3d). The contact angle is greatly reduced from 39.6° to 7.10° upon the inclusion of an ultrathin Al_2O_3 interface layer.

3.2. Effect of SiNPs Height on Cell Performance. The height of the SiNPs plays an important role in device performance. The current−voltage characteristics of the SiNP/PEDOT:PSS hybrid solar cells having different nanopillar heights were measured under 100 mW/cm^2 illumination. Five cells were fabricated for each value of the silicon nanopillar height and their electrical performance was measured. Figure 4 depicts the average value of short circuit current density (J_{SC}), open circuit voltage (V_{OC}), fill factor (FF), and power conversion efficiency (PCE) of the fabricated devices as a function of SiNP height. The measured value of short circuit current density for the fabricated SiNP/PEDOT:PSS solar cells increases with the increase in nanopillar height, reaching a maximum of 29.5 mA/cm^2 at SiNP height of 0.4 μm (see Figure 4a), beyond which it decreases quasi-linearly to 21.2 mA/cm^2 as height is further increased to 1.2 μm. Similar effects have also been observed by Shiu et al.[14] and He et al.[19] The unique antireflection property of the SiNP array textured surface is directly reflected in the measured value of J_{SC} of the SiNP/PEDOT:PSS solar cell. The maximum J_{SC} of 29.5 mA/cm^2 for an SiNP array textured cell with SiNP height of 0.4 μm is almost 36.6% greater than a planar/PEDOT:PSS cell. On the other hand, the measured open circuit voltage of the SiNP/PEDOT:PSS solar cells was observed to decrease continuously from a maximum value of 538 mV to a minimum of 490 mV as the SiNP height varied from 0.2 to 1.2 μm (see Figure 4a). This can be attributed to an increased junction recombination with increases in surface area. The power conversion efficiency of the SiNP/PEDOT:PSS solar cells produced, reached a maximum value of 9.65%, for a nanopillar height of 0.4 μm, which compares favorably to the 7.02% observed for a planar/PEDOT:PSS cell. This is mainly due to the increase in short circuit current density and fill factor for the device, despite the slight decrease in V_{OC}. A promising fill factor value of 62 was achieved for a SiNP/PEDOT:PSS hybrid cell which also compares favorably to FF of 60 for a planar/PEDOT:PSS solar cell. This could be attributed to an increased carrier separation due to the increased junction area. Furthermore, the SiNP/PEDOT:PSS heterojunction provides a shorter pathway for the minority charge carriers toward the respective electrode. The measured photovoltaic parameter of the proposed hybrid solar cells are summarized in Table 1. Compared to the schemes employing random SiNWs, an SiNP array has enough spacing between the pillars for conformal coating employing PEDOT:PSS without the addition of other organic molecules (see Supporting Information Figure S1). Furthermore, one of the major drawbacks of SiNW/PEDOT:PSS hybrid devices resides on the wire length, thus, the longer they are the more difficult it is for the PEDOT:PSS to coat every wire conformally, completely, and uniformly to form the required core shell structure. Frequently, pinhole regions are created that

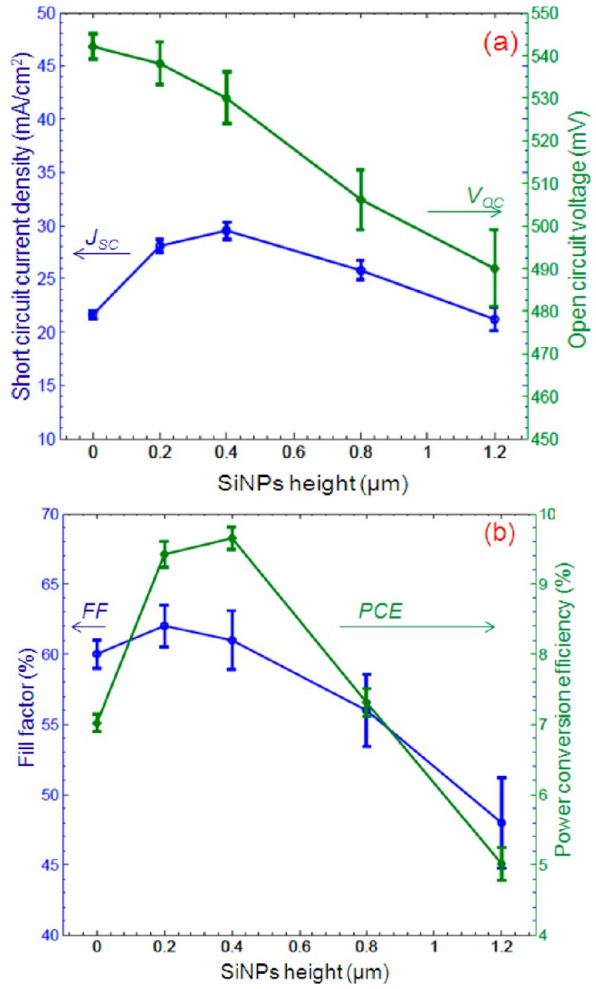

Figure 4. Average photovoltaic performance parameters of (a) J_{SC} and V_{OC} and (b) FF and PCE of the SiNP/PEDOT:PSS solar cell as a function of SiNP height.

Table 1. Average Photovoltaic Properties of the Hybrid SiNP/PEDOT:PSS Solar Cells with Different SiNP Heights

cell types	V_{OC} (mV)	J_{SC} (mA/cm^2)	FF (%)	PCE (%)[a]
planar/PEDOT:PSS	542	21.6	60.1	7.02 ± 0.12
0.2 μm SiNP/PEDOT:PSS	538	28.1	62.0	9.42 ± 0.18
0.4 μm SiNP/PEDOT:PSS	530	29.5	61.2	9.65 ± 0.16
0.8 μm SiNP/PEDOT:PSS	506	25.8	56.2	7.31 ± 0.20
1.2 μm SiNP/PEDOT:PSS	490	21.2	48.0	5.01 ± 0.23

[a]The statistics present the error range of five measured samples with 95% confidence interval.

dx.doi.org/10.1021/am402598j | ACS Appl. Mater. Interfaces 2013, 5, 9620−9627

form a local shunt, which ultimately deteriorate the V_{OC} and FF of the device.

To further investigate the influence of SiNP height on the PV performance of the fabricated devices, the external quantum efficiency (EQE) of the SiNP/PEDOT:PSS solar cells with different pillar heights was measured and the corresponding graphs are shown in Figure 5. The measured EQE improves

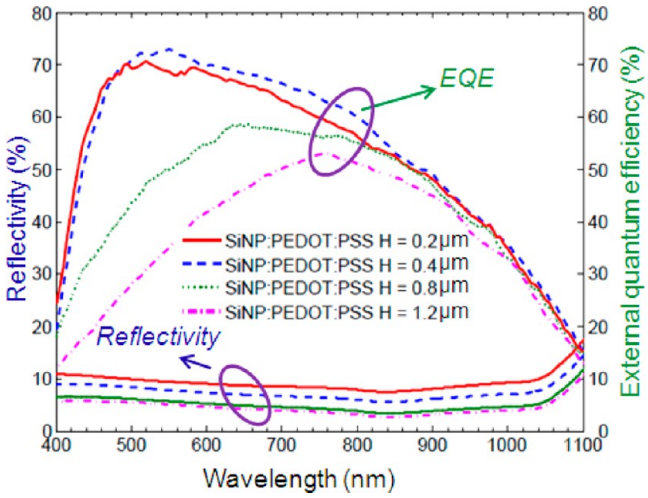

Figure 5. Reflectivity spectra (%) and measured external quantum efficiency (%) of the SiNP/PEDOT:PSS hybrid solar cells with different SiNP height.

with the increase in SiNP height up to 0.4 μm due to light trapping effects. However, beyond 0.4 μm the EQE decreases drastically with increases in SiNP height, despite of their effective light trapping (see the reflectance spectra in Figure 5), especially in the wavelength range of 400−800 nm. This can be attributed to increases in carrier recombination with the increase in SiNP height. The SiNPs with taller pillar heights fabricated by the metal assisted chemical etching method produce more surface defects, resulting in shorter carrier lifetime and, therefore, a higher carrier recombination velocity. Since most of the short wavelengths photons are absorbed in a few tenths of nanometer of silicon, the most drastic drop in EQE is observed at those wavelengths for devices with a larger height, while there is no significant change for wavelengths >800 nm, as most of the long wavelength photons are absorbed in the bulk region of the device. This suggests that an effective surface passivation (junction passivation) is inevitable to improve the electrical performance of SiNP/PEDOT:PSS solar cells.

3.3. Effect of Al_2O_3 Passivation Layer on Cell Performance. One factor limiting the efficiency of SiNP/PEDOT:PSS hybrid cell is the low carrier collection efficiency due to increased surface recombination, in spite of having better light absorption characteristics. The open circuit voltage of a SiNP/PEDOT:PSS solar cells, irrespective of pillar height, is observed to be smaller compared to their planar/PEDOT:PSS counterparts. To reduce the recombination at the nanotextured silicon surface with a SiNP/PEDOT:PSS structure, we employed an ultrathin (<1 nm) ALD Al_2O_3 as an interface passivation layer. ALD Al_2O_3 was chosen as a passivation layer due to its unique chemical and field effect passivation characteristics, as well as the ability of ALD to deposit high quality, conformal films on high aspect ratio features, with an angstrom-level control of the film thickness at low temperatures. Different samples were prepared, with increases in the thickness of the Al_2O_3 interface layer and its effects on photovoltaic performance was measured. The height of the SiNPs was fixed at 0.4 μm. Figure 6 shows

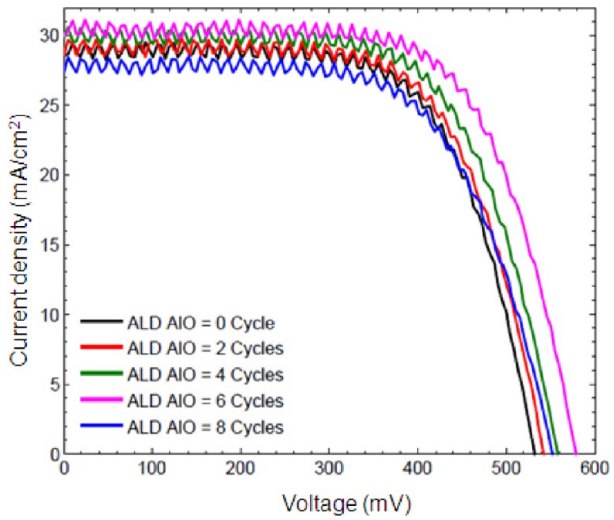

Figure 6. Current density versus voltage characteristic curves for SiNP/PEDOT:PSS hybrid solar cells with increases in the number of cycles during the deposition of the ALD Al_2O_3 interfacial layer. The height of the SiNPs was fixed at 0.4 μm.

the curves of current density versus voltage characteristic for SiNP/PEDOT:PSS hybrid solar cells with increases in the number of the ALD cycles during the deposition of the Al_2O_3 interfacial layer. The average photovoltaic performance of the SiNP/ALD−Al_2O_3/PEDOT:PSS hybrid solar cells is summarized in Table 2. It was found that the power conversion

Table 2. Influence of ALD Al_2O_3 Interface Layer Thickness on the Photovoltaic Performance of the SiNP/PEDOT:PSS Solar Cells

cell types	V_{OC} (mV)	J_{SC} (mA/cm^2)	FF (%)	PCE (%)[a]
SiNP/0C-ALD/PEDOT:PSS	530	29.5	61.2	9.65 ± 0.16
SiNP/2C-ALD/PEDOT:PSS	546	29.2	60.9	9.72 ± 0.14
SiNP/4C-ALD/PEDOT:PSS	557	29.8	59.2	9.79 ± 0.15
SiNP/6C-ALD/PEDOT:PSS	578	30.1	59.8	10.56 ± 0.14
SiNP/8C-ALD/PEDOT:PSS	552	28.2	58.3	9.02 ± 0.17
SiNP/10C-ALD/PEDOT:PSS	524	26.4	54.6	7.51 ± 0.23

[a]The statistics present the error range of five measured samples with 95% confidence interval.

efficiency of the devices increased with increases in the thickness of the Al_2O_3 interface layer, reached its maximum value of 10.56% for six cycles ALD Al_2O_3, while the PCE of the same device without Al_2O_3 was 9.65%. This can be attributed mainly to the increased open circuit voltage of the device. The maximum open circuit voltage of 578 mV was achieved for the six-cycle ALD Al_2O_3, which is ∼9.1% higher compared to the same device without Al_2O_3 interface layer. The maximum short circuit current density of the cell with the Al_2O_3 barrier layer was 30.1 mA/cm^2 compared to 29.5 mA/cm^2 for a cell without

dx.doi.org/10.1021/am402598j | ACS Appl. Mater. Interfaces 2013, 5, 9620−9627

Al_2O_3 despite the slight decrease in FF. Further increases in thickness of the Al_2O_3 layer have a deleterious effect in device performance especially due to increases in the series resistance (increases in the insulation barrier for the carriers) which ultimately has an adverse effect on V_{OC}, J_{SC}, and FF of the device. The Al_2O_3 layer in SiNP/Al_2O_3/PDEOT:PSS structure also prevents the oxidation of Si. The performance of the proposed device with an ultrathin ALD Al_2O_3 barrier layer was observed to remain unaltered after 72 h of exposure to ambient, while the corresponding device without the ALD Al_2O_3 layer degraded significantly (see Supporting Information Table S1). This can be attributed to be due to a thicker native oxide film grown at the interface between Si and the PEDOT:PSS layer, which imposes an increased barrier height for the carriers to be collected.

The V_{OC} value of the SiNP/PEDOT:PSS sample with an optimized ALD Al_2O_3 interface layer (~578 mV) compares favorably to values reported for SiNW/PEDOT:PSS hybrid solar cells.[19,21] High V_{OC} values usually need a careful interface preparation for effective carrier collection, which is commonly not associated with defective interfaces. For the ideal diode model (n = 1), the Shockley equation for V_{OC} can be expressed as[22]

$$V_{OC} = \frac{nk_BT}{q}\ln\left(\frac{J_{SC}}{J_O} + 1\right) \quad (1)$$

Where, J_O is the saturation current density, and n, k_B, T, and q are diode ideality factor, Boltzmann constant, absolute temperature, and elementary charge, respectively. We believe the slight increase in J_{SC} (~0.6 mA/cm^2) for a SiNP/PEDOT:PSS solar cell with an optimized Al_2O_3 barrier layer does not sufficiently warrant the relatively large increase in V_{OC} (~57 mV) observed. Assuming a similar J_O for both SiNP/PEDOT:PSS solar cells with and without Al_2O_3 barrier layer, the increase in J_{SC} would lead to a V_{OC} gain defined by the equation

$$\Delta V_{OC} = \frac{k_BT}{q}\ln\left(\frac{J_{SC}w/\mathrm{ALD}}{J_{SC}wo/\mathrm{ALD}}\right) \quad (2)$$

Using this relation, we anticipated a V_{OC} gain of ~1 mV, which is smaller than the experimentally measured voltage gain. Ostensibly, the assumption of a constant J_O is not warranted. To further investigate the underlying reasons for the observed voltage gain, we measured and graphed the dark current density versus voltage characteristics of the hybrid SiNP/PEDOT:PSS solar cells with and without Al_2O_3 interface layer. The observations indicate that the dark current density is suppressed significantly after employing the ultrathin Al_2O_3 barrier layer (see Figure 7). From the best fitting of the dark J–V characteristic curves at the forward bias condition, we extracted the values of saturation current density (J_O) and diode ideality factor (n), which is defined by the relation,

$$\ln(J) = \ln(J_0) + \left(\frac{q}{nk_BT}\right)V \quad (3)$$

We obtained the value of J_O to be 0.48 μA/cm^2 for a SiNP/PEDOT:PSS hybrid cell with an Al_2O_3 barrier layer, which was lower than that of a cell without a barrier layer, namely, 2.19 μA/cm^2. The ideality factors of 2.06 and 2.21, respectively, were obtained for the SiNP/PEDOT:PSS cells with and without the Al_2O_3 barrier layer. Using J_{SC} = 30.1 mA/cm^2, J_O = 0.48 μA/cm^2, and n = 2.06, for the fabricated SiNP/PEDOT:PSS solar cells with Al_2O_3 barrier layer, and employing those values in eq 1, we obtain a V_{OC} of 592 mV, which falls within 2.4% of the experimentally observed value of 578 mV. The reduction in the dark current is thought to provide evidence for a reduced carrier recombination with improved junction quality. However, the fill factor of the device is relatively low compared to other pure inorganic photovoltaic devices. We calculated the ideal FF of the SiNP/PEDOT:PSS hybrid solar cells in the absence of series and shunt resistances using the equation defined by[38]

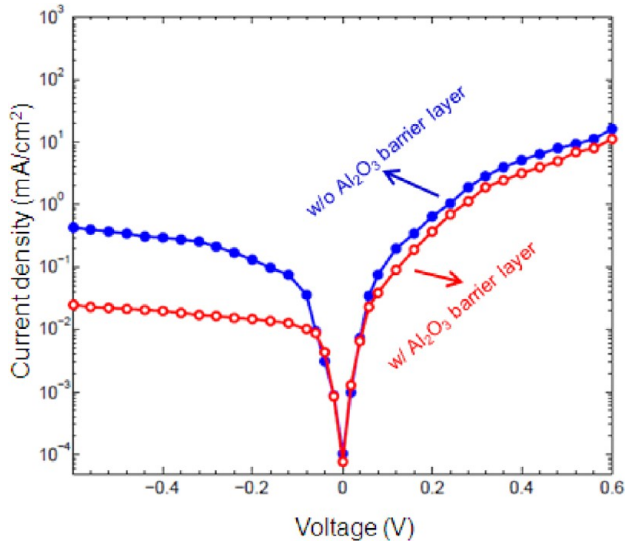

Figure 7. Dark J–V characteristic curves for SiNP/PEDOT:PSS hybrid solar cells with and without (open circles) an Al_2O_3 interface layer. The height of the SiNPs was fixed at 0.4 μm.

$$\mathrm{FF} = \frac{v_{oc} - \ln(v_{oc} + 0.72)}{v_{oc} + 1} \quad (4)$$

Where $v_{oc} = V_{OC}/(nk_BT/q)$ is the normalized open circuit voltage. Using V_{OC} = 578 mV and n = 2.06, we obtain the ideal FF of ~71% for the proposed hybrid device compared to the measured FF of 60%. This suggests that there is a significant electrical loss due to the parasitic series and shunt resistances of the device. The electrical loss can be suppressed by forming an ohmic contact on both the front and the rear sides of the device. This could be accomplished by forming a back surface field on the rear side of the device and creating a metal grid electrode on the front. Hence, we believe that there is still room to improve the electrical performance of the proposed hybrid device.

4. CONCLUSIONS

A promising hybrid solar cell device based on highly ordered silicon nanopillar (SiNP) arrays and poly(3,4-ethylenedioxythiophene):polystyrenesulfonate (PEDOT:PSS) has been described. Relatively simple, low temperature processing methods were employed for the fabrication of the proposed solar cell. The effect of SiNP height on the solar cell performance of the device was investigated. The PCE of a SiNP/PEDOT:PSS hybrid cell with an optimized SiNP height of 0.4 μm was observed to be 9.65%. With the utilization of an ultrathin ALD deposited Al_2O_3 junction passivation layer, we

observed a short circuit current density and an open circuit voltage as high as 30.1 mA/cm^2 and 578 mV, respectively, which led to a PCE value in excess of 10.56%. An ideal fill factor of ~71% was calculated for the hybrid device described herein which is significantly higher than the measured value of ~60%. Thus, there is a noticeable electrical loss in the proposed device. Further investigation is needed to fully explore the proposed hybrid SiNP/PEDOT:PSS hybrid solar cell.

■ ASSOCIATED CONTENT

Supporting Information

Figure S1: cross-sectional SEM image of PEDOT:PSS coated SiNP array. Figure S2: EDX spectra obtained at the interface of the Al_2O_3 film and Si substrate. Table T1: photovoltaic performance parameters of SiNP/PEDOT:PSS hybrid solar cells with and without Al_2O_3 passivation layer after 72 h exposure in air. This material is available free of charge via the Internet at http://pubs.acs.org.

■ AUTHOR INFORMATION

Corresponding Author

*Phone: 210-458-6562. E-mail: pbz620@my.utsa.edu.

Notes

The authors declare no competing financial interest.

■ ACKNOWLEDGMENTS

We thank Dr. Mike Gerhold, Technical Manager of the U.S. Army Research Office, for the financial support provided for this project (ARO grant number W911NF-13-1-0110). This project was also supported by a grant from the National Institute on Minority Health and Health Disparities (G12MD007591) from the National Institutes of Health. The authors would also like to acknowledge for the Ferro Corporation, CA, USA, for technical support.

■ REFERENCES

(1) Aberle, A. G.; Altermatt, P. P.; Heiser, G.; Robinson, S. J.; Wang, A.; Zhao, J.; Krumbein, U.; Green, M. A. *J. Appl. Phys.* **1995**, *77* (7), 3491−3504.
(2) Zhao, J.; Wang, A.; Green, M. A.; Ferrazza, F. *Appl. Phys. Lett.* **1998**, *73*, 1991−1993.
(3) Garnett, E.; Yang, P. *Nano Lett.* **2010**, *10*, 1082−1087.
(4) Oh, J.; Yuan, H.-C.; Branz, H. M. *Nat. Technol.* **2012**, *7*, 743−748.
(5) Hoth, C. N.; Schilinsky, P.; Choulis, S. A.; Brabec, C. J. *Nano Lett.* **2008**, *8*, 2806−2813.
(6) Zhao, G.; He, Y.; Li, Y. *Adv. Mater.* **2010**, *22*, 4355−4358.
(7) He, F.; Yu, L. *J. Phys. Chem. Lett.* **2011**, *2*, 3102−3113.
(8) Kim, J. Y.; Lee, K.; Coates, N. E.; Moses, D.; Nguyen, T. Q.; Dante, M.; Heeger, A. J. *Science* **2007**, *317*, 222−225.
(9) Mei, J.; Ogawa, K.; Kim, Y.-G.; Heston, N. C.; Arenas, D. J.; Nasrollahi, Z.; McCarley, T. D.; Tanner, D. B.; Reynolds, J. R.; Schanze, K. S. *ACS Appl. Mater. Interfaces* **2009**, *1*, 150−161.
(10) Seo, J. H.; Gutacker, A.; Sun, Y.; Wu, H.; Huang, F.; Cao, Y.; Scherf, U.; Heeger, A. J.; Bazan, G. C. *J. Am. Chem. Soc.* **2011**, *133*, 8416−8419.
(11) Liu, C.-Y.; Holman, Z. C.; Kortshagen, U. R. *Adv. Func. Mater.* **2010**, *20*, 2157−2158.
(12) Liu, C.-Y.; Holman, Z. C.; Kortshagen, U. R. *Nano Lett.* **2009**, *9*, 449−452.
(13) He, L.; Jiang, C.; Rusli; Lai, D.; Wang, H. *Appl. Phys. Lett.* **2011**, *99*, 021104(1)−021104(3).
(14) Shiu, S.-C.; Chao, J.-J.; Hung, S.-C.; Yeh, C.-L.; Lin, C.-F. *Chem. Mater.* **2010**, *22*, 3108−3113.
(15) Huynh, W. U. *Science* **2002**, *295*, 2425−2427.
(16) Avasthi, S.; Lee, S.; Loo, Y.-L.; Sturm, J. C. *Adv. Mater.* **2011**, *23*, 5762−5766.
(17) Wright, M.; Uddin, A. *Sol. Energy Mater. Sol. Cells* **2012**, *107*, 87−111.
(18) Wu, F.; Cui, Q.; Qiu, Z.; Liu, C.; Zhang, H.; Shen, W.; Wang, M. *ACS Appl. Mater. Interfaces* **2013**, *5*, 3246−3254.
(19) He, L.; Jiang, C.; Wang, H.; Lai, D.; Rusli. *ACS Appl. Mater. Interfaces* **2012**, *4*, 1704−1708.
(20) Lu, W.; Wang, C.; Yue, W.; Chen, L. *Nanoscale* **2011**, *3*, 3631−3634.
(21) Jeong, S.; Garnett, E. C.; Wang, S.; Yu, Z.; Fan, S.; Brongersma, M. L.; McGehee, M. D.; Cui, Y. *Nano Lett.* **2012**, *12*, 2971−2976.
(22) Pietsch, M.; Bashouti, M. Y.; Christiansen, S. *J. Phys. Chem. C* **2013**, *117*, 9049−9055.
(23) Zhu, Y.; Song, T.; Zhang, F.; Lee, S.-T.; Sun, B. *Appl. Phys. Lett.* **2013**, *102*, 113504(1)−113504(4).
(24) Lu, W.; Chen, Q.; Wang, B.; Chen, L. *Appl. Phys. Lett.* **2012**, *100*, 023112(1)−023112(4).
(25) Bashouti, M. Y.; Pietsch, M.; Brönstrup, G.; Sivakov, V.; Ristein, J.; Christiansen, S. *Prog. Photovolt.: Res. Appl.* **2013**, http://dx.doi.org/10.1002/pip.2315.
(26) Khatri, I.; Tang, Z.; Liu, Q.; Ishikawa, R.; Ueno, K.; Shirai, H. *Appl. Phys. Lett.* **2013**, *102*, 063508(1)−063508(5).
(27) Moiz, S. A.; Nahhas, A. M.; Um, H.-D.; Jee, S.-W.; Cho, H. K.; Kim, S.-W.; Lee, J.-H. *Nanotechnol.* **2012**, *23*, 145401(1)−145401(7).
(28) Han, S. E.; Chen, G. *Nano Lett.* **2010**, *10*, 1012−1015.
(29) Yang, T.-C.; Huang, T.-Y.; Lee, H.-C.; Lin, T.-J.; Yen, T.-J. *J. Electrochem. Soc.* **2012**, *159*, B104−B108.
(30) Pudasaini, P. R.; Ayon, A. A. *Opt. Commun.* **2012**, *285*, 4211−4214.
(31) Christesen, J. D.; Zhang, X.; Pinion, C. W.; Celano, T. A.; Flynn, C. J.; Cahoon, J. F. *Nano Lett.* **2012**, *12*, 6024−6029.
(32) Pudasaini, P. R.; Elam, D.; Ayon, A. A. *J. Phys. D: Appl. Phys.* **2013**, *46*, 235104(1)−235104(8).
(33) Zhang, F.; Sun, B.; Song, T.; Zhu, X.; Lee, S. *Chem. Mater.* **2011**, *23*, 2084−2090.
(34) He, L.; Jiang, C.; Wang, H.; Lai, D.; Rusli. *Appl. Phys. Lett.* **2012**, *100*, 073503(1)−073503(3).
(35) Cheung, C. L.; Nikolić, R. J.; Reinhardt, C. E.; Wang, T. F. *Nanotechnol.* **2006**, *17*, 1339−1343.
(36) Mikhael, B.; Elise, B.; Xavier, M.; Sebastian, S.; Johann, M.; Laetitia, P. *ACS Appl. Mater. Interfaces* **2011**, *3*, 3866−3873.
(37) Pudasaini, P. R.; Ayon, A. A. *Microelecrtron. Eng.* **2013**, *110*, 126−131.
(38) Green, M. A. *Sol. Cells* **1982**, *7*, 337−340.